JOURNAL OF Applied Polymer SCIENCE

Graphene Nanoplatelet-Polyetherimide Composites: Revealed Morphology and Relation to Properties

Huang Wu, Lawrence T. Drzal
Composite Materials and Structures Center, Michigan State University, East Lansing, Michigan 48824
Correspondence to: H. Wu (E-mail: huang.wu.84@gmail.com)

ABSTRACT: In this research, a novel sample preparation technique was applied to reveal the morphology exfoliated graphene nanoplatelets [GNP, ~10 nm thick and ~5 μm in diameter)] and Polyetherimide (PEId) nanocomposite and study the relationship between processing and properties. The morphology of nanoscale fillers used to be hard to capture through conventional sample preparation. The polish-plasma etching approach presented in this article successfully created contrast between filler and matrix. As a result, distribution and orientation of the fillers were obtained to study the effect of injection molding, compression molding and annealing. It was found that the orientation was significantly different depending on processing routes. The information obtained from morphology study also led to the modification of Tandon–Weng model, resulting in improved prediction of elastic modulus of the composite. The SEM images also clearly revealed change of filler orientation after annealing. © 2013 Wiley Periodicals, Inc. J. Appl. Polym. Sci. 130: 4081–4089, 2013

KEYWORDS: morphology; microscopy; nanotubes; graphene and fullerenes; mechanical properties; nanostructured polymers

Received 2 May 2013; accepted 15 June 2013; Published online 8 July 2013
DOI: 10.1002/app.39678

INTRODUCTION

Polymer nanocomposites usually refer to a polymer matrix filled by high-surface-area reinforcing fillers[1] including carbon nanotubes (CNTs), carbon nanofibers, nanoclay, carbon black (CB), graphene platelets, and so on. Since their discovery, nanoparticles were expected to function as substitute reinforcements for conventional reinforcement fibers because of the theoretically high particle properties and the significant improvement in nanocomposite properties attained at low loadings. Furthermore, significant advantages were expected from gains in processing by eliminating the need for layer-by-layer assembly or autoclave processing. The functionality of the nanofillers is highly dependent on their morphology. For example, as conductive fillers, the zero-dimensional CB can improve composite electrical conductivity as a result of electrical percolation at low (~5%) loading for nonpolar, low crystallinity thermoplastics,[2] while high aspect ratio CNT filled composites with a similar matrix have a percolation threshold of 0.1 vol %.[3] The high aspect ratio and linear shape of CNTs make it easier to form a percolated network with more contacts being formed between filler particles. Two-dimensional (nanoplatelet) fillers such as alumino-silicate nanoclay can also produce composites with low gas permeability, which cannot be achieved by CNTs or CB because of the highly tortuous path formed by their two-dimensional nature.[4,5] Research also suggests that this kind of filler can also be used to improve the fire retardancy of its composite.[6]

Given the importance of the morphology of nanocomposites, it is critical to finding a consistent and reliable way to reveal it. Modern microscopic techniques have given researchers various ways to observe the morphology for microscale devices and materials. Scanning electron microscope (SEM) and transmission electron microscope (TEM) are the most widely used techniques. SEM is useful for checking the fracturing surface of a composite. However, when the size of the filler particle is in hundreds of nanometers to a few micrometers range, it is hard to distinguish between the filler morphology and the toughness generated by the polymer matrix. TEM is extremely useful to investigate the dispersion state of nanofillers such as nanosilicate,[7,8] CNT.[9,10] However, only a small portion of the sample can be observed at one time, making it difficult to understand the overall condition of the fillers throughout the entire sample.

This research focused on developing an effective method to reveal the morphology of nanocomposites in order to obtain information such as filler orientation, which is key to explaining the performance of the composite. Exfoliated graphite nanoplatelets (GNPs)/polyether imide (PEId) composite is studied. As demonstrated in Drzal's group,[11] GNPs consisting of small stacks of graphene can be fabricated by acid intercalation, microwave heating, and ultrasonication pulverization and be scaled inexpensively into quantity production by this route. The size and thickness of GNP is controllable during fabrication. Typical sizes of the platelets range from submicrometer to 25

μm in diameter usually notated as GNP-1, GNP-5, and GNP-15 where the number refers to the average statistical diameter with thicknesses in the 5–10 nm range.

Because of the two-dimensional nature of GNP and its high aspect ratio, final properties of GNP based nanocomposites can vary due to the processing methods selected. For example, the molding processes are important for their ability to make complex shaped integrated composites. Kim and Macosko[12] have shown that differences in electrical conductivity of polycarbonate/graphene composites can be attained depending on whether they were made by injection molding or compression molding. Compression molded samples showed much better electrical conductivity than injection molded ones. Mohanty et al.[13] found that postmolding treatment, such as annealing after injection molding can provide better flexural modulus and strength and alter the morphology of nanocomposites and thus their properties. Dynamic percolation behavior of CB composites has been studied by Wu et al.[14] who found that due to Brownian motion, CB particles are able to reposition themselves locally under high temperature during which the viscosity of the polymer matrix is low. Particles of platelet shape such as alumino-silicates and graphene, might not be subject to Brownian motion because of their larger dimensions. Researchers have shown faster particle reorganization in layered alumino-silicate/polymer composites than expected as compared to Brownian motion theory.[15–17] The real driving force might be the elastic restoring force of the polymeric matrix generated during processing though no widely-accepted conclusion has been drawn yet. Kim and Macosko proposed a disorientation mechanism for graphene composites based on X-ray scattering and rheology data, pointing out that at low loadings (<3 wt %) of graphite filler, the rotation experienced by the particles caused by annealing still cannot increase particle contact with each other, while at high loadings (>12 wt %), the movement of filler particles is restricted due to excluded volume interactions between particles.

PEId has drawn a lot of attention due to its extremely low flammability and excellent chemical and heat resistance. The addition of carbon nanofillers into PEId has been applied to grant the material with multifunctionality such as electrical[18] and thermal conductivities. Ghose et al.[19] studied the effect of multiple carbon nanofillers on the mechanical properties and thermal conductivity of PEId composite and showed importance of particle alignment. Kumar et al.[20] used synergistic effect of combining GNP and CNT to gain a percolation threshold at 0.5 wt % on a solution casted film. However, most methods are either hard to scale up due to the cost of expensive nanofiller (CNT) or process (solution-based), or need high loading (40 wt %) of graphite based filler to achieve significant improvement. Moreover, although most researchers are aware of the importance of morphology-property relationship for this system, the lack of an effective imaging technique hindered the interpretation, especially because of the surface roughness generated during fracturing the sample. In this research, the morphology of the GNP/polyetherimide (PEId) nanocomposites was successfully revealed and linked to the processing method and the properties. Melt-extrusion in a twin-screw extruder was used to compound GNP and PEId pellets, which were either injection molded or compression molded. Annealing under confinement at the molding temperature (340°C) was investigated for its effect on mechanical and electrical properties. The SEM images based on the new sample preparation technique are presented to explicitly show the morphology-property relation for the system. Tandon–Weng equation was modified according to morphology study and the prediction of composite elastic modulus was improved.

EXPERIMENTAL

Materials

PEId (Ultem 1010) was provided by Sabic Americas, Inc. (Houston, TX). GNP-5 was provided by XG Sciences. (East Lansing, MI, http://xgsciences.com) with an average diameter of 3.9 μm and a specific surface area of 40 $m^2\ g^{-1}$.

Melt-Extrusion

Melt-extrusion was carried on a Leistritz co-rotating twin-screw extruder (MIC27/6L-48D) with a screw length/diameter of 40: 1. Barrel temperatures were set to 310°C with a melt temperature at 340°C. The die pressure was ~5.5 MPa. Screw speed was set at 150 rpm.

Molding

After extrusion compounding, part of the composite material was compression molded in a CARVER Laboratory Press (Model 2731, Fred S. Carver). A picture-frame mold was used with a dimension of 76 × 76 × 3.3 mm^3. The material was heated up to 340°C and held for 15 min. A compression pressure of 20 MPa was applied to the material and was held for 15 min. After that, the press was cooled with water. The other part of the composite material was injection molded with a Milacron VSX 85-4.44 (Cincinnati, OH) injection molder with a Master Precision tensile specimen die (Series No. 24157, Greenville, MI). The melt pressure during injection molding was 90 MPa. The central part of the injection molded tensile bars were cut into a 12.7 × 12.7 mm^2 and annealed in a mold of the same size under a pressure of 23 MPa at 340°C for 1 h.

Characterization

The resistance of GNP/PEId composites was measured in two directions by a two probe Femtostat (Gamry Instrument): the "through-plane direction," which through the specimen thickness and was the same direction as the applied pressure in compression molding while the "in-plane direction," which in the direction of flow in the injection molded specimen and was perpendicular to the pressure in the compression molded specimen. The resistance value was then converted into resistivity by taking into account the sample dimensions. Flexural strength and modulus were tested under ASTM 790 standard on a UTS SFM-20 machine (United Calibration) at room temperature. The test was performed at a flexural rate of 0.03 in min^{-1}. According to ASTM 790 standard, the sample strain should not exceed 5% during flexural test, so the strength value was calculated from the force at 5% strain if the sample had not failed before that. The morphology of the nanocomposites was observed by SEM (JSM-6400, Jeol, Tokyo, Japan). To investigate the distribution and orientation of the fillers, the tensile bar

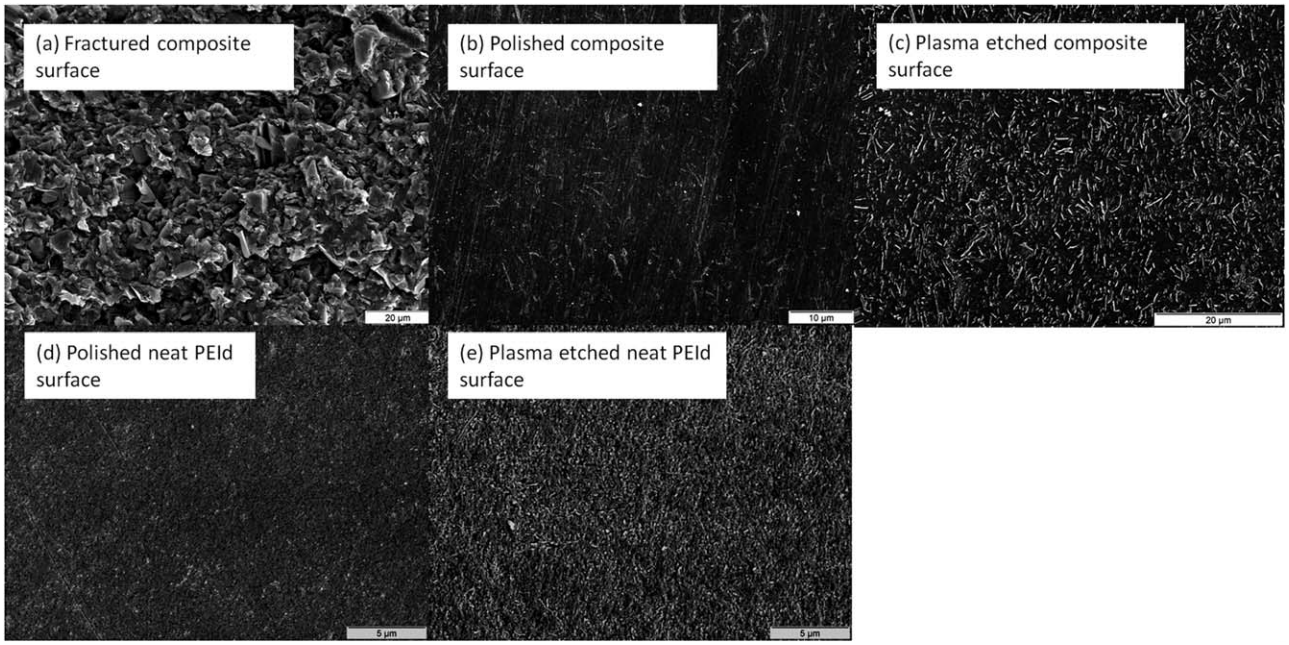

Figure 1. Comparison between fractured, polished, and plasma etched surfaces. Images were taken from GNP/PEId composites and neat PEId.

specimens were cut along as well as perpendicular to the material flow direction as in injection molding. After cutting, the to-be-observed surface was attached to aluminum substrate by double-sided tape. A plastic ring holder was placed around the sample. Epoxy was filled into the holder and cured under room temperature. The sample-embedded epoxy puck was then polished by SiC with #4000 grit finish. One micrometer and 0.05 μm alumina powder/water slurry were used consecutively for further polishing. Oxygen plasma was used after the final polishing to etch away a layer of polymer in order to expose the GNP particle. The polished-and-plasma treated surface was then sputter coated with gold.

RESULTS AND DISCUSSION

Effect of Sample Preparation for SEM

The comparison between SEM images taken from a fractured surface, a polished surface and a plasma etched surface is shown in Figure 1. Compared with un-etched surfaces, the plasma treated one shows best contrast between GNP particles and the matrix. On the fractured surface [Figure 1(a)], it is hard to distinguish GNP particles from the matrix because of the roughness of the sample. On the polished surface [Figure 1(b)], some GNP particles can be seen (short white lines), but the contrast is not good, and a lot of smaller particles are invisible due to the entrapment of polymer matrix. Also, the polishing pattern (long parallel straight lines) is present that may interfere with the interpretation of the morphology. In Figure 1(c), on the plasma etched surface, the white lines stand for the cross-section of the GNP particles. The dark part is occupied by the matrix. The contrast between GNP particles and the matrix is better than the polished surface. Plus, more particles are revealed. As a comparison, the polished and plasma etched neat PEId resin surface morphologies are shown in Figure 1(d,e). It can be seen that the plasma treatment created some surface roughness by etching away polymer. However, the contrast between GNP particles and matrix is high enough in Figure 1(c) that the interpretation of the morphology is not affected by the small level of surface roughness created by resin etching.

It is important to point out that the plasma etching would also result in the size reduction of GNP particles, as indicated by Lu et al.[21] and Paredes et al.[22] The O_2 plasma preferentially etch the edge of the GNP particles much faster than the basal plane as reported by Paredes et al. However, in our study, the etching effect on graphite can be neglected. First, the height reduction of the GNP particles is much slower than that of the matrix, which results in good contrast between filler and matrix as indicated in the SEM images. Second, the size reduction of the particles caused by the etching from the radius direction of the particles is not significant, as indicated by the contact between the tip of the GNP and the matrix in Figure 1. It is believed that the GNP particle tips exposed in the SEM images were originally covered by the matrix. The O_2 plasma etched away the matrix at a much faster rate than it did to the tip of GNP, exposing larger portion of GNP than the part it etched away.

Kalaitzidou et al.[23] developed a novel method to fabricate GNP nanocomposites by coating the GNP particles onto polymer powder surface (precoating process). After compression molding, the coated structure forms a continuous GNP phase and helps the electrical percolation. In their work, the fractured surface was used to demonstrate the coated structure. However, it is hard to interpret due to surface roughness. Figure 2 shows the comparison between the fractured surface adapted from Ref. 23 and the plasma etched surface for the sample made from the same process. In this process, GNP particles are coated

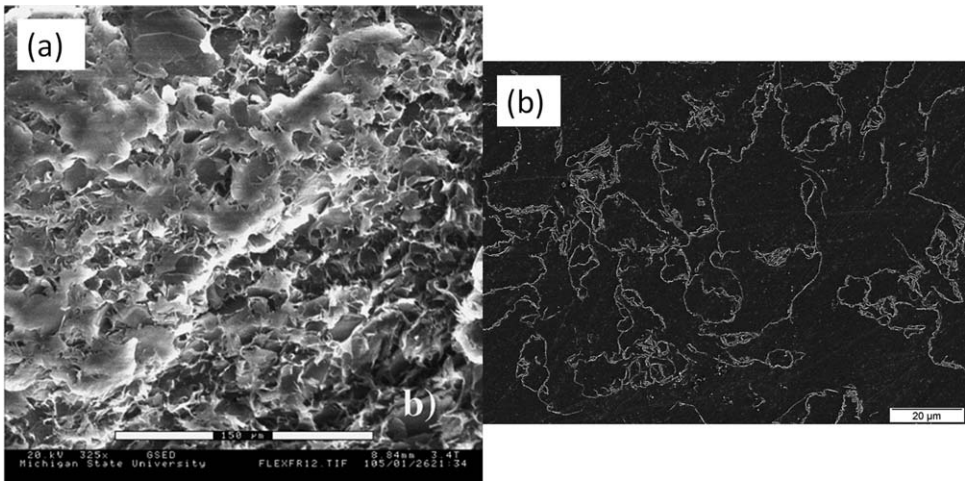

Figure 2. Comparison between fractured surface and plasma etched surface for precoated composite (a) fractured surface of GNP/PP, adapted from Ref. 23 and (b) plasma etched surface of GNP/PEId.

on polymer powder. When the coated powder is compression molded, long continuous GNP phases are formed. Figure 2(a) is the fractured surface of the composite made from precoating. It suffers from a mixed morphology of GNP particles and the roughness of the matrix, resulting in indirect indication of the formation of the continuous GNP phase. On the contrary, in Figure 2(b), the white lines represent GNP. It is explicitly shown that the continuous phase of the GNP is formed.

Morphology of GNP/PEId Composites

Generally speaking, compression molding results in non or low preferential alignment of anisotropic fillers. In Figure 3(a), the cross-section of the compression molded GNP/PEId composite is observed. The GNP particles (white lines) are overall randomly oriented in the PEId matrix (black background) with slight preferential alignment perpendicular to compression direction.

The orientation of the GNP particles in the injection molded specimens is much more complicated because of the material flow and the walls of the mold. The injection molded specimens show anisotropic behavior due to material flow. GNP orientation should be present at in two cross-sections: one surface perpendicular to the flow direction and the other one along the flow direction [Figure 3(b,c)]. In Figure 2(b), different orientations of the GNP particles can be seen at different position of the cross-section. The portion of the sample that is close to the wall has almost perfect orientation parallel to it due to the large shear rate in this location. A change of orientation can be observed at the corner due to the confinement of the wall of the mold. As the distance between the particle and the wall increase, the GNP particle undergoes less orientation. This is because viscous melt of the composite has the highest shear rate at the wall and the lowest at the center of the specimen.

Compression Molding Versus Injection Molding

The flexural modulus/strength and electrical resistivity of the GNP-5/PEId composites made from compression molding and injection molding are shown in Figure 4. Generally, compared to the injection molded samples, the compression molded ones showed lower electrical resistivity and lower mechanical modulus/strength, the electrical percolation threshold of which is around 3 wt % for the through-plane direction and 1 wt % for the in-plane direction. This is the result of the GNP particles having a slightly preferential alignment direction because of the compressive force during molding as shown in Figure 3(a). The electrical resistivity of the injection molded samples is much higher than the compression molded ones. It is found that in the through-plane direction, the GNP particles do not percolate even at 10 wt % loading. For the in-plane direction, the 10 wt % sample shows percolated behavior, but the resistivity is two orders of magnitude higher than its compression molded counterpart.

The flexural modulus of the compression molded composites is increased by 70%, while that the injection molded ones is increased by 100%. The strength of the injection molded specimens increases steadily with the increase of GNP loading up to 5 wt % while at 10 wt % it remains at the same level as the neat polymer. However, a decrease is recorded after 3 wt % loading for compression molded samples. Interestingly, 3 wt % loading is around the electrical percolation threshold, suggesting the forming of a continuous filler phase is producing strength reducing defects in the composite. The orientation of the filler particles leads to differences in the mechanical behavior between the compression and injection molded samples. In Figure 4(c), the modulus of the GNP-5/PEId composites made from injection molding is higher than the ones made from compression molding. For flexural strength [Figure 4(d)], no significant difference is observed between injection and compression molded samples up to 3 wt % of GNP loading. However, at above 5 wt %, compression molded samples exhibit lower strength than the injection molded ones.

The key to explain the different performance between compression molded and injection molded samples is their morphologies. As shown in Figure 5(a), the particles are randomly oriented. The connection between particles is good. However, in Figure 5(b), most of the particles are aligned. The alignment not only prevents the particles from connecting with each other

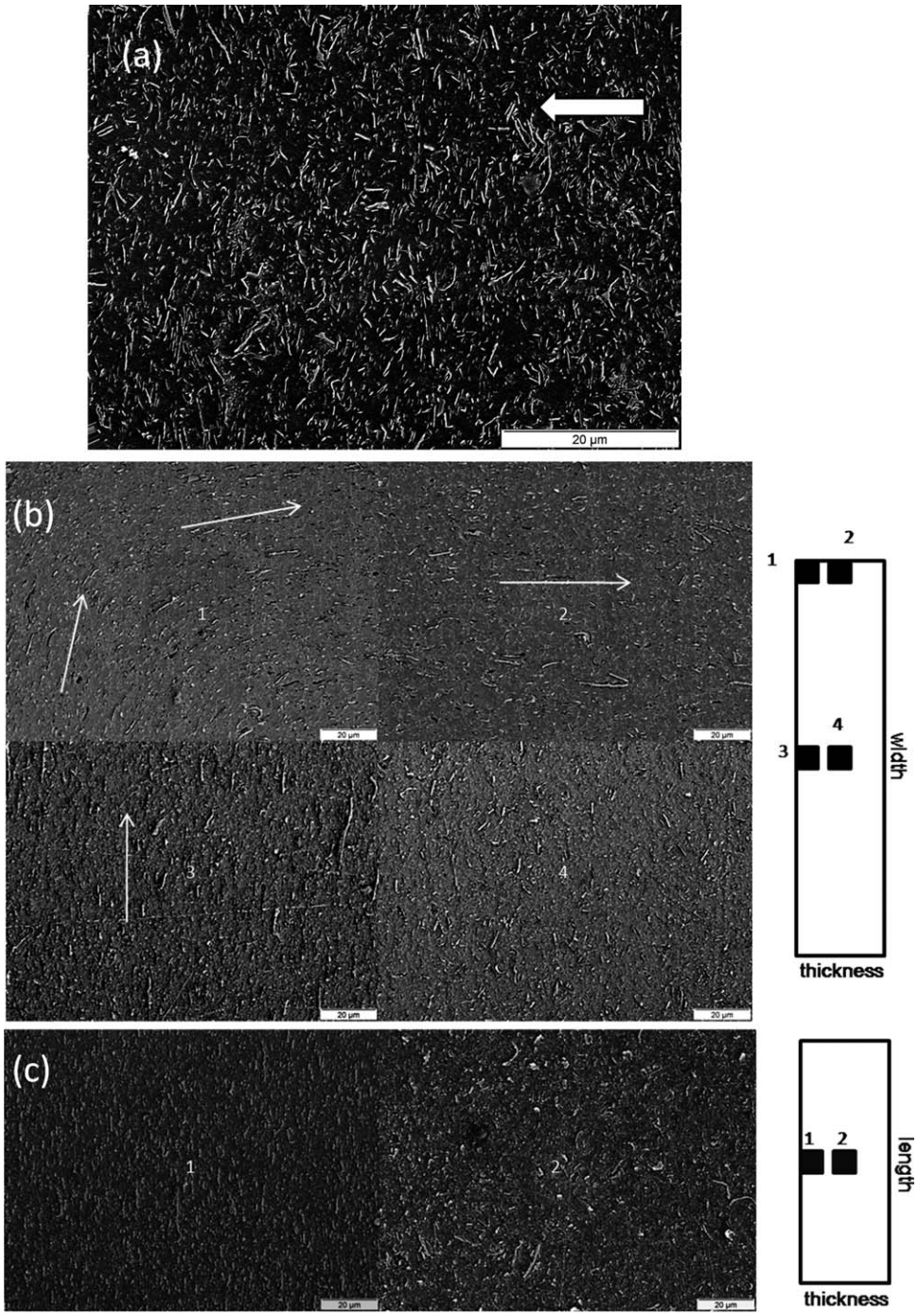

Figure 3. Orientation of GNPGNP particles observed on: (a) cross-section of a compression molded specimen (arrow showing compression direction); (b) the cross-section of an injection molded specimen perpendicular to the flow direction and (c) along the flow direction (the scale bar represents 20 μm).

in the through-plane direction, but also places the particles apart in the in-plane direction, preventing the formation of a continuous conductive filler phase and resulting in higher resistivity. The effect of particles alignment on modulus will be discussed in the next section.

Model Prediction of Modulus

Because of the complicated orientation situation of GNP/PEId composites, its not easy to predict their mechanical behavior. Figure 6(a) shows the calculated modulus value of the composites using the Tandon–Weng equation.[24]

$$\frac{E_{11}}{E_m} = \frac{1}{1+\phi(-2\upsilon_m A_3+(1-\upsilon_m)A_4+(1+\upsilon_m)A_5 A)/2A} \quad (1)$$

In eq. (1), E_{11}, Em, are the Young's modulus of the composite and neat matrix polymer, respectively. ϕ is the volume fraction of the filler, υ_m is the Poisson's ratio of the matrix, A and A_i are functions of ϕ, υ_m, and Eshelby's tensor.

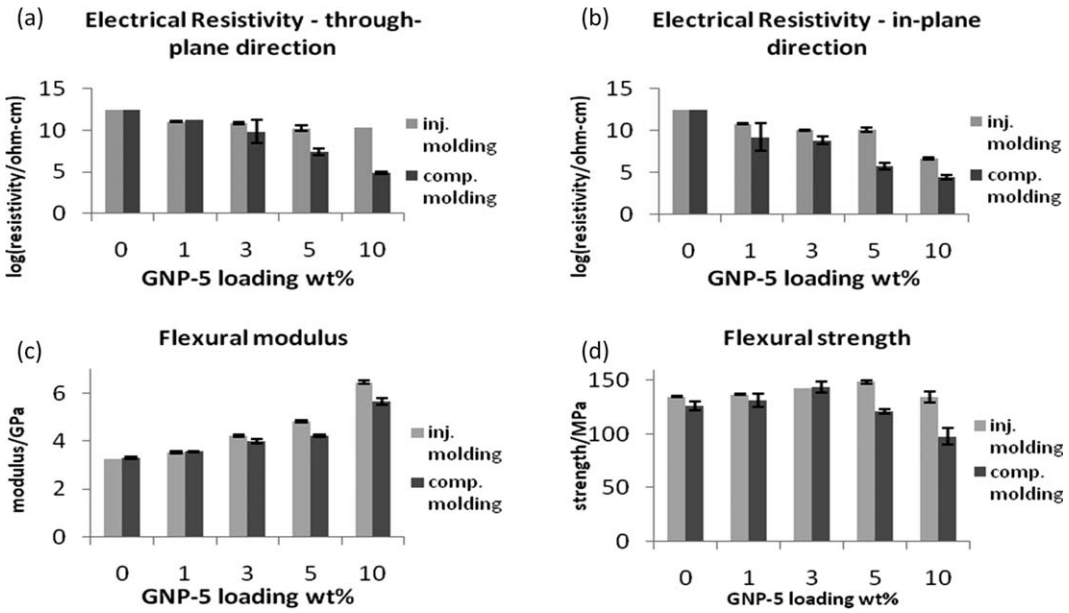

Figure 4. Comparison between GNP-5/PEId composites made from injection molding and compression molding.

Tandon and Weng gave formulas for both unidirectional and randomly oriented[25] situations. The values of the parameters used in the equation are listed in Table I.

The aspect ratio of the GNP particles after processing can be determined by the following equation[29]:

$$A_f = \frac{3\phi_{sphere}}{2\phi_{platelet}} \tag{2}$$

Where $\phi_{\text{sphere}} = 0.29$, which is the percolation threshold of spherical-shaped conductive fillers.[30] From Figure 1(a,b), the electrical percolation takes place around 2 wt %. From eq. (2), the actual aspect ratio of the GNP particles should be 35.

Interestingly, if we consider the surface area of the GNP prior to processing and the average size of the particles, the expected aspect ratio should be around 160. However, during melt-extrusion, these platelet-shaped particles are reduced in lateral dimension because of the mechanical shearing of the twin-screws (Figure 7).

The SEM image (Figure 7) shows an average diameter of GNP particles after processing as 0.96 μm, about 4 times smaller than the starting material, resulting in an average aspect ratio of 40. This result is consistent with the result calculated from eq. (2).

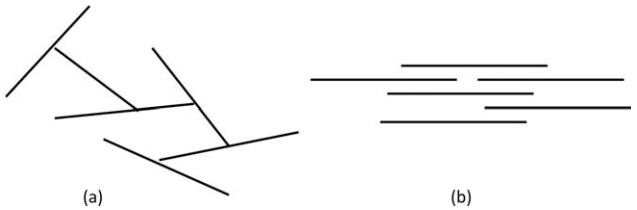

Figure 5. Schematics of alignment situation of GNP particles in PEId matrix: (a) random orientation after compression molding, (b) aligned orientation after injection molding.

It is worthy to point out that the reduction in particle size is not favored for this type of material, since the aspect ratio of the GNP particle plays an important role in most properties of the composite. However, the melt-extrusion condition process used in this study was not optimized to preserve the particle size.

In Figure 6, the random platelet orientation Tandon–Weng equation predictions underestimate the modulus of the compression molded GNP/PEId composites. While for injection molded samples, unidirectional model overestimates the modulus. The cause of the mismatch lies in the orientation of the particles, which is revealed by SEM images. The particles in the compression molded samples are not completely randomly oriented [Figure 3(a)], while in the injection molded samples, the particles are not perfectly aligned either [Figure 3(c)]. To simplify the problem, we only analyze the orientation along the flow direction, which is also the direction of tensile testing.

From Figure 3(c), the particles close to the surface of the sample tend to orient in the flow direction while the ones at the center of the specimen tend to be randomly oriented. This phenomenon suggests a combination of the unidirectional model and the random model:

$$\frac{E_{11}}{E_m} = x\frac{E_{11,\ unidirectional}}{E_m} + (1-x)\frac{E_{11,\ random}}{E_m} \tag{3}$$

where x stands for the average degree of orientation:

$$x = 1.5\left(\overline{a_{11}} - \frac{1}{3}\right) \tag{4}$$

$\overline{a_{11}}$ is the average orientation factor throughout the thickness of a specimen. $\overline{a_{11}} = 1$ represents 100% orientation while $\overline{a_{11}} = 1/3$ represents 0% orientation. To calculate $\overline{a_{11}}$, SEM images were taken at the cross-section of flow direction from edge to center

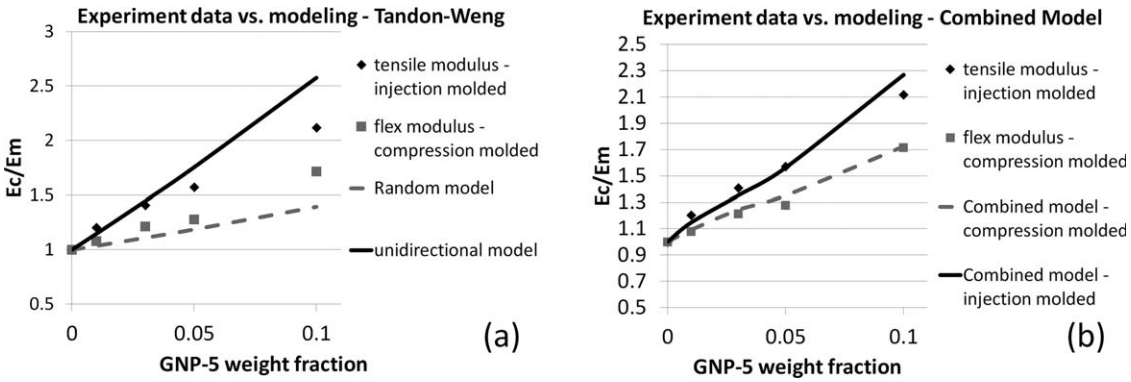

Figure 6. Comparison between experimental modulus and Tandon-Weng modeling.

Table I. Parameters Used in Tandon-Weng Equation

Component	Modulus (GPa)	Poisson's Ratio	Density (g/cm^3)
GNP	1060[26,27]	0.2[28]	2.1
PEId	3.3	0.36	1.29

(sample thickness: 3.3 mm). The SEM images were processed in Image-Pro Plus software (Media Cybernetics, MD) to calculate the orientation information, a_{11} of the particles:

$$a_{11} = < cos^2\theta > \quad (5)$$

where θ is the angle between the GNP basal plane and the flow direction.

Figure 8 shows the change of degree of orientation from the surface to the center of the sample. Although none of the points reaches the extreme value for either unidirectional ($a_{11} = 1$) or completely random ($a_{11} = 1/3$), it is clear that the sample can be split into two parts with different levels of orientation. At close to the surface, the GNP particles are mostly aligned along the flow direction in injection molding, while at the center of the sample the particles tend to be more randomly oriented.

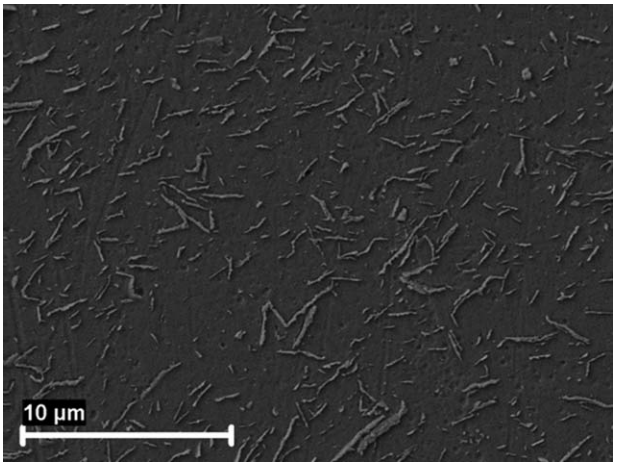

Figure 7. SEM image of 5 wt % GNP-5/PEId composite made from melt-extrusion, showing reduced particle size (original average size: 3.9 μm in diameter).

This observation is consistent with literature.[31] The average values based on different positions in a specimen for 3, 5, and 10 wt % are 0.72, 0.66, and 0.74, respectively. For compression molded specimens, the corresponding x-values are 0.40, 0.29,

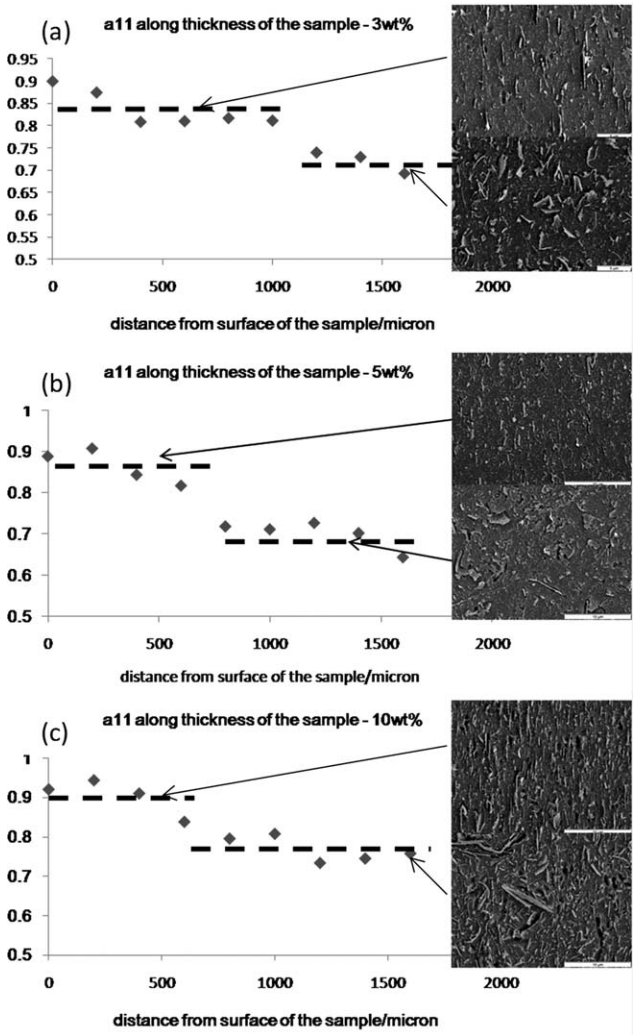

Figure 8. a_{11} along the thickness direction on the cross-section plane of flow direction (diamond series are a_{11} values and dash lines indicate the distinguish of two regions) and the representative morphology (scale bars represent 5 μm).

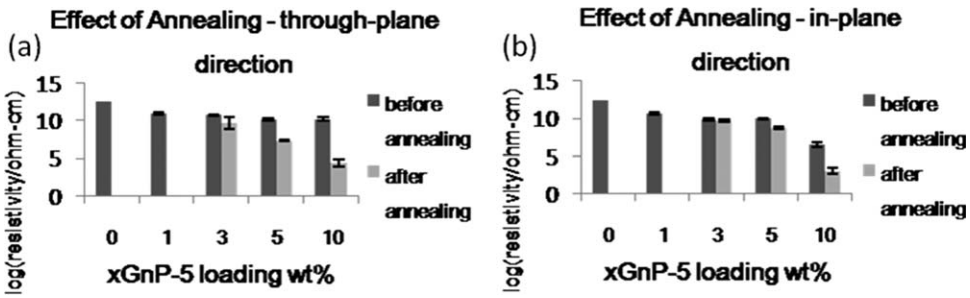

Figure 9. Effect of annealing on electrical resistivity.

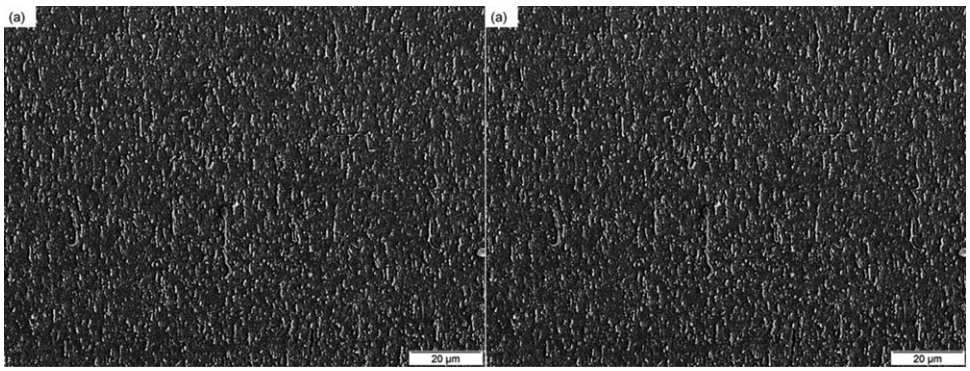

Figure 10. Five weight percent GNP-5/PEId composite (a) before annealing and (b) after annealing. Images were taken along the flow direction (as during injection molding), showing the morphology of the near-surface part of the tensile bar specimen.

and 0.28 for 3, 5, and 10 wt %, respectively. The model prediction based on eq. (3) and its comparison with the experimental data are shown in Figure 6(b). It can be seen that the agreement between the combined model and experimental data is much improved as compared to unmodified Tandon–Weng model.

Effect of Annealing

It has been shown that the percolation behavior of nanocomposites filled with conductive nanoparticles is influenced by annealing under high temperature (above the melt temperature of the matrix polymer). Similarly during annealing, GNP particles are able to reorient due to polymer chain relaxation and elastic restoring force.[12]

From Figure 9, the electrical resistivity in the through-plane direction decreases significantly after annealing. The 5 wt % GNP-5/PEId composite displays percolation. In the in-plane direction, the decrease in electrical resistivity is less than in the through-plane direction, but is significant. A 1.5 order of magnitude decrease is attained for the 5 wt% loading and a 2.5 order of magnitude decrease for the 10 wt% loading.

SEM images of the composites taken both before and after annealing document the GNP reorientation. Figure 10 shows the morphology comparison between the composites before and after annealing. It is found that the area that is close to the surface of the tensile bar has a higher degree of orientation [Figure 10(a)]. However, after annealing, the highly aligned orientation is destroyed as shown in Figure 10(b). As discussed earlier, less oriented particles have a better chance to connect with each other (Figure 5) and therefore provide path for electrical conductivity. The fact that the decrease of resistivity in the through-plane direction is larger than that in the in-plane direction indicates that the movement of the particles does not result in their aggregation in the flow direction. The particles rotate at the original position rather than move along the flow direction.

Figure 11 shows the change of electrical resistivity of GNP/PEId composites along with the annealing time. For the 5 wt % sample, the minimum time for the effect of annealing to affect the percolation point is between 40 and 60 min. For the 10 wt % sample, the time is around 10 min. With higher GNP loadings, the annealing percolation time decreases. This is due

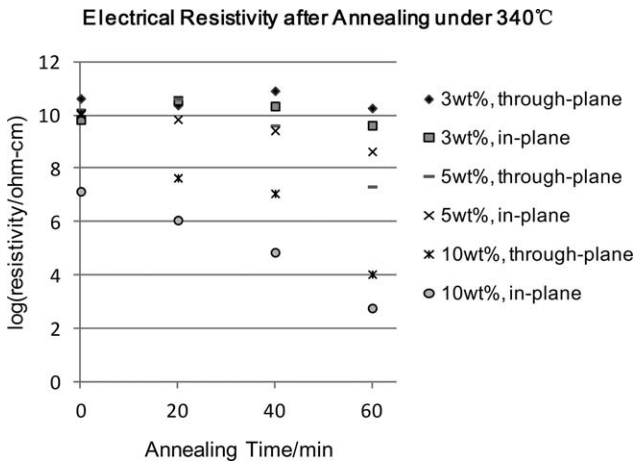

Figure 11. Time dependence of the annealing effect.

to the smaller distance between GNP particles in the composites as the concentration increases. Composites with higher loadings of GNP have a shorter distance between particles, requiring less movement of the particles to make contact with each other.

CONCLUSIONS

Polishing—plasma etching process was developed for preparing SEM samples. The contrast created between filler and matrix helped reveal the distribution and orientation of the nanofillers explicitly. GNP and PEId were compounded by melt-extrusion followed by either injection molding or compression molding. It was found that injection molding leads to better mechanical properties while compression molding results in better electrical conductivity. When the Tandon–Weng equation was applied to predict the modulus of the samples, it was found that the random particle orientation Tandon–Weng equation under estimates compression molded samples while unidirectional model overestimates injection molded samples. A combined model based on the overall average degree of orientation fits both compressions molded and injection molded samples well. Annealing is found to be effective in overcoming the orientation effects caused by molding and leads to higher electrical conductivity of the GNP/PEId composites as a result of the rotation of GNP particles during the high temperature annealing treatment. SEM images of GNP morphology in the molded specimens confirm the nanoplatelet orientation and annealing effects and support these conclusions.

ACKNOWLEDGMENTS

The authors would like to thank The Boeing Company for sponsoring this project and also Mr. Gregg Bogucki for his help.

REFERENCES

1. Vaia, R. A.; Giannelis, E. P. *MRS Bull.* **2001**, *26*, 394.
2. Huang, J. C. *Adv. Polym. Technol.* **2002**, *21*, 299.
3. Bauhofer, W.; Kovacs, J. Z. *Compos. Sci. Technol.* **2009**, *69*, 1486.
4. LeBaron, P. C.; Wang, Z.; Pinnavaia, T. *J. Appl. Clay Sci.* **1999**, *15*, 11.
5. Kim, J. K.; Hu, C. G.; Woo, R. S. C.; Sham, M. L. *Compos. Sci. Technol.* **2005**, *65*, 805.
6. Porter, D.; Metcalfe, E.; Thomas, M. J. K. *Fire Mater.* **2000**, *24*, 45.
7. Giannelis, E. P. *Appl. Organomet. Chem.* **1998**, *12*, 675.
8. Lan, T.; Pinnavaia, T. *J. Chem. Mater.* **1994**, *6*, 2216.
9. Tang, W. Z.; Santare, M. H.; Advani, S. G. *Carbon* **2003**, *41*, 2779.
10. Ginic-Markovic, M.; Matisons, J. G.; Cervini, R.; Simon, G. P.; Fredericks, P. M. *Chem. Mater.* **2006**, *18*, 6258.
11. Fukushima, H. In Department of Chemical Engineering and Materials Science; East Lansing: Michigan State University, **2003**.
12. Kim, H.; Macosko, C. W. *Polymer* **2009**, *50*, 3797.
13. Mohanty, A. K.; Wibowo, A.; Misra, A.; Drzal, L. T. *Compos. Part A: Appl. Sci. Manufact* **2004**, *35*, 363.
14. Wu, G. Z.; Asai, S.; Zhang, C.; Miura, T.; Sumita, M. *J. Appl. Phys.* **2000**, *88*, 1480.
15. Schmidt, G.; Nakatani, A. I.; Butler, P. D.; Karim, A.; Han, C. C. *Macromolecules* **2000**, *33*, 7219.
16. Solomon, M. J.; Almusallam, A. S.; Seefeldt, K. F.; Somwangthanaroj, A.; Varadan, P. *Macromolecules* **2001**, *34*, 1864.
17. Ren, J. X.; Casanueva, B. F.; Mitchell, C. A.; Krishnamoorti, R. *Macromolecules* **2003**, *36*, 4188.
18. Sawai, P.; Banerjee, S. *J. Appl. Polym. Sci.* **2008**, *109*, 2054.
19. Ghose, S.; Working, D. C.; Connell, J. W.; Smith, J. G.; Watson, K. A.; Delozier, D. M.; Sun, Y. P.; Lin, Y. *High Perform. Polym.* **2006**, *18*, 961.
20. Kumar, S.; Sun, L. L.; Caceres, S.; Li, B.; Wood, W.; Perugini, A.; Maguire, R. G.; Zhong, W. H. *Nanotechnology* **2010**, *21*, 105702.
21. Lu, X. K.; Huang, H.; Nemchuk, N.; Ruoff, R. S. *Appl. Phys. Lett.* **1999**, *75*, 193.
22. Paredes, J. I.; Martinez-Alonso, A.; Tascon, J. M. D. *Langmuir* **2007**, *23*, 8932.
23. Kalaitzidou, K.; Fukushima, H.; Drzal, L. T. *Compos. Sci. Technol.* **2007**, *67*, 2045.
24. Tandon, G. P.; Weng, G. *J. Polym. Compos.* **1984**, *5*, 327.
25. Tandon, G. P.; Weng, G. *J. Compos. Sci. Technol.* **1986**, *27*, 111.
26. Ren, J. X.; Silva, A. S.; Krishnamoorti, R. *Macromolecules* **2000**, *33*, 3739.
27. Shante, V. K. S.; Kirkpatr, S. *Adv. Phys.* **1971**, *20*, 325.
28. Gupta, M.; Wang, K. K. *Polym. Compos.* **1993**, *14*, 367.
29. Blakslee, O. L. *J. Appl. Phys.* **1970**, *41*, 3373.
30. Lee, C.; Wei, X. D.; Kysar, J. W.; Hone, J. *Science* **2008**, *321*, 385.
31. Cho, J.; Luo, J. J.; Daniel, I. M. *Compos. Sci. Technol.* **2007**, *67*, 2399.